Multiplexed Time-Correlated Single-Photon Counting

D. J. S. Birch,[1] D. McLoskey,[1] A. Sanderson,[1] K. Suhling,[1] and A. S. Holmes[1]

We review the technique of multiplexed time-correlated single-photon counting whereby multiple fluorescence decay curves are recorded in parallel by statistically time-sharing a single time-to-amplitude converter. Application of the multiplexing technique to measuring the fluorescence lifetime topography of a self-absorbing sample is demonstrated. Further possibilities are discussed for multiplexed optical fiber sensor networks with built-in intelligence for detecting and discriminating between different metal ions in solution.

INTRODUCTION

The time-correlated single-photon counting (TCSPC) technique is the most widely used method of measuring fluorescence decay times [1,2]. Advantages of TCSPC include a wide dynamic range, known data statistics (Poisson) and data weights, a conveniently digitized data format, visual display of kinetics, and high time resolution. However, TCSPC is quite inefficient insofar as the fluorescence count rate detected must be kept to a few percent of the excitation repetition rate to avoid data pileup [1,2]. Although this pileup limitation is inconvenient in principle, it is rarely a problem in practice due to the high repetition rate of present day flashlamp and laser sources. A much more fundamental limitation concerns the implementation of TCSPC, which, by and large, addresses only one small fraction of the available fluorescence contour. The fluorescence decay signature of a sample, F, can be expressed generally in terms of a data surface, e.g.,

$$F = F(I, \lambda_F, t, \underline{p}, \underline{r}) \tag{1}$$

where I is the emission intensity, λ_F the fluorescence wavelength, t time, $\underline{p}$ polarization, and $\underline{r}$ the spatial location.

[1] Department of Physics and Applied Physics, University of Strathclyde, Glasgow G4 0NG, Scotland, UK.

The larger the fraction of the available data surface which can be addressed in a single measurement, the higher is the measurement specificity. Most present-day TCSPC fluorometers are simplexed instruments, e.g., decay curves are recorded at one fluorescence wavelength at a time which is clearly inefficient given the much greater data surface available. In recent years we have developed parallel processing technology which enables a much greater fraction of the fluorescence data surface to be recorded simultaneously using TCSPC and which overcomes the usual pileup limitation.

In multiplexed TCSPC (MUX-TCSPC) each detection channel is associated with its own timing discriminator and memory segment of a multichannel analyzer (MCA) just as in the usual simplexed approach. In MUX-TCSPC the "stop" signals from the multiple detection channels are combined to provide an unsorted mixture of signals to the stop input of the time-to-amplitude converter (TAC). The TAC conversion events which then follow are sorted into different segments of the MCA memory by using the timing discriminator output from each channel to initiate logic levels which address the appropriate MCA memory segment for each channel. Coincident stop events in more than one channel are rejected by inhibiting the TAC conversion if they occur within an enable time window determined by the TAC range. Consequently each channel can be operated at the

usual pileup limit and hence the data acquisition rate is enhanced proportionately, subject to reject events. We have developed unique electronics for multiplexing/routing time-correlated signals and demonstrated its use in a wide range of applications. Initially we applied the multiplexing technique to simultaneous acquisition of fluorescence and excitation (SAFE) [3,4] using two detection channels. Subsequently we extended multiplexing to three channels, primarily for use in anisotropy studies, such that two orthogonal planes of polarization in a T-format and the excitation pulse could be measured simultaneously [5,6]. Extension to four channels enabled for the first time single-photon decay measurements to be made simultaneously across a fluorescence spectrum using a polychromator [7,8]. More recently we have demonstrated the multiplexing of fluorescence signals down optical waveguides using multianode microchannel plate photomultiplier detection as a step toward acquiring data from distributed sensor networks [9,10]. All the early multiplexing work was based on TTL logic circuitry, which from the standpoints of cost, reliability, and physical size, limits the maximum number of channels at which MUX-TCSPC is practicable to little more than four channels.

This paper describes the application of our current state of the art in MUX-TCSPC, which is based on a custom-designed integrated circuit capable of handling up to 16 channels. It must be emphasized that the MUX-TCSPC techniques we have developed are quite different from techniques reported previously for sequential measurements, for example, the alternate collection of different planes of fluorescence polarization to correct for intensity drifts [11] and the alternate collection of excitation and decay to correct for temporal drifts [12,13]. Our approach is also different from using an optical (or electronic) delay to separate time-correlated signals acquired in the same memory segment [14,15]. Unlike our approach, none of these other techniques make any inroads into the pileup limitation, nor do they enhance data acquisition rate by performing measurements in parallel.

The MUX-TCSPC technique we have developed is the most efficient approach to single-photon timed decay measurements yet demonstrated. By the addition of suitable detection optoelectronics and one multiplexing-routing module containing the customized IC, a conventional simplexed TCSPC system can be given a 16-fold enhancement in measurement capacity. Our technique is quite general and can be used with both laser and spark sources operated in forward or reversed "start" – "stop" coincidence and is compatible with most MCAs, TACs, and timing discriminators. Any single-photon timing detector can be used including the conventional photo-

multiplier, avalanche photodiode, and microchannel plate photomultiplier. In addition to applications in anisotropy and multiwavelength measurements, MUX-TCSPC has potential uses in high-performance liquid chromatography, single-photon timing measurements with low-repetition rate sources, e.g., N_2 lasers, and fluorescence microscopy. Here we describe the application to spatially resolved fluorescence kinetics.

MULTIPLEXING THEORY

Figure 1 shows the general multiplexing scheme for m single-photon timing channels. In the case of 16 channels a four-bit TTL routing logic code is sent to the MCA to select the appropriate memory segment in which to store the TAC conversion, e.g., 0000 for segment 1, 1111 for segment 16, etc.

If the rate of single-photon pulses detected in one channel is S_p (the "stop" rate), then for a source repetition rate S_t (the "start" rate).

$$S_p/S_t = \alpha \qquad (2)$$

Usually count rates are chosen to give a ratio α of ~ 0.01 to avoid pileup distortion caused by only the first stop event being detected in each TAC cycle.

In the case of m single-photon timing channels, in the form of either an array or discrete detectors, let us first assume that the probability of detecting a fluorescence photon is the same for each channel, i.e., α is constant. This simplifies the mathematical detail such that the key features of the statistical behavior become clearer. Obviously, when measuring decays at multiple fluorescence wavelengths with a polychromator, this assumption is unlikely to be valid but the multiplexing theory can in principle be expanded to take account of this.

For m channels the probability of k channels containing single-photon pulses per excitation is given by the probability of detecting photons in k detectors multiplied by the probability of detecting no photons in the other detectors [16], i.e., a binomial-type distribution.

$$P_k(m) = \frac{m!}{k!(m-k)!} (\alpha)^k (1 - \alpha)^{m-k} \qquad (3)$$

with the total rate of stop pulses arriving at the TAC, S_p^T, then being given by

$$S_p^T = S_t \sum_{k=1}^{m} kP_k(m) = S_t m\alpha \qquad (4)$$

For example, in the case of a 16-channel array the probabilities of there being no pulses, one pulse, and more
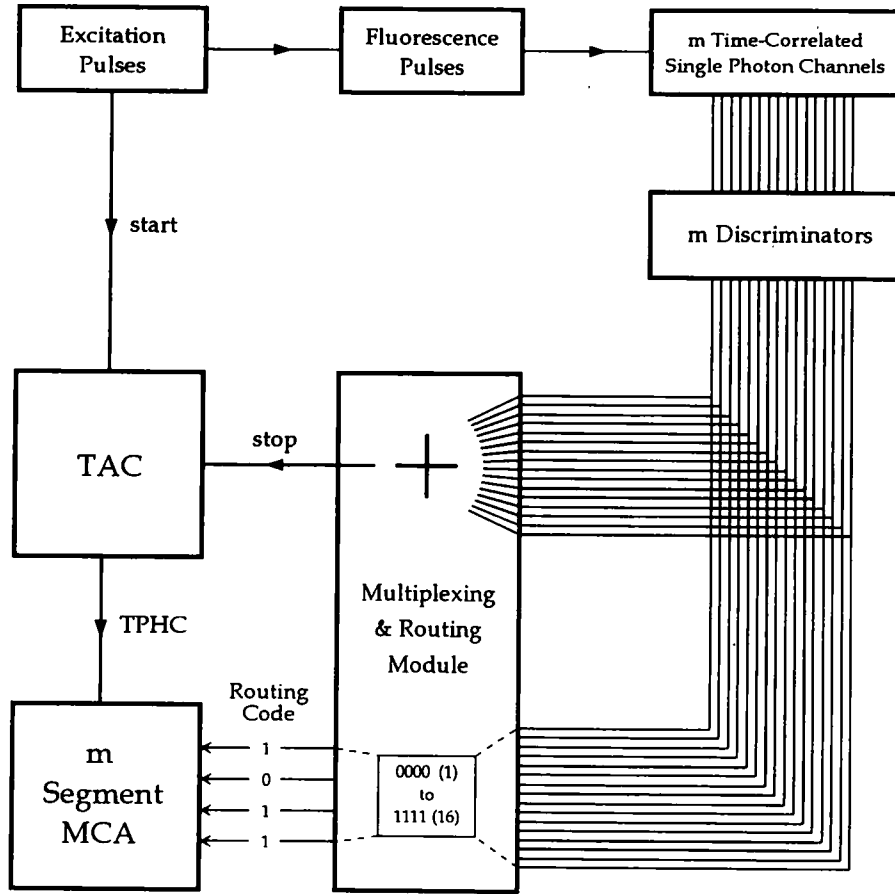
Fig. 1. Multiplexed time-correlated single-photon counting.

than one pulse in the channels per start pulse are given, respectively, by

$$P_0 \,(16) = (1 \,-\, \alpha)^{16} \qquad (5)$$

$$P_1 \,(16) = 16\alpha(1 \,-\, \alpha)^{15} \qquad (6)$$

$$P_{>1} \,(16) = 1 \,-\, (1 \,-\, \alpha)^{16} \,-\, 16\alpha(1 \,-\, \alpha)^{15} \qquad (7)$$

The total rate of coincident pulses output from the TAC will be lower than that given by Eq. (4) because of the necessity to reject coincident events occurring in more than one channel. $P_{>1}(m)$ describes the probability of multiple events, and $P_{>1}(m)S_t$ the associated reject rate. As a consequence of the above it can be seen that the maximum overall probability of obtaining a TAC output is that given by the probability of detecting a coincident pulse in just one channel, i.e.,

$$P_1 \,(m) \,=\, m\alpha(1-\alpha)^{m-1} \qquad (8)$$

Equation (8) thus provides the generalized form of the statistical theory for multiplexed single-photon timing ex-

periments where m detection channels share a single TAC and coincident pulses in two or more channels are rejected. The usual simplexed expressions $P_1(1) = \alpha$ for a single channel $(m=1)$ is thus a special case of Eq. (8). The maximum rate of stop pulses converted by the TAC S_p^c is then given by

$$S_p^c \,=\, S_t m\alpha(1 \,-\, \alpha)^{m-1} \qquad (9)$$

and reject rate S_p^r given by

$$S_p^r \,=\, S_t \,[1 \,-\, (1-\alpha)^m \,-\, m\alpha(1-\alpha)^{m-1}] \qquad (10)$$

The reject given by Eq. (10) is a form of data pileup which we call cross-channel pileup and arises only in multiplexed measurements because of the need to identify unambiguously the stop channel causing each TAC conversion. It is the presence of the reject rate which causes the overall rate of TAC conversions to be less than $S_t m\alpha$, the rate of stop pulses arriving at the TAC.

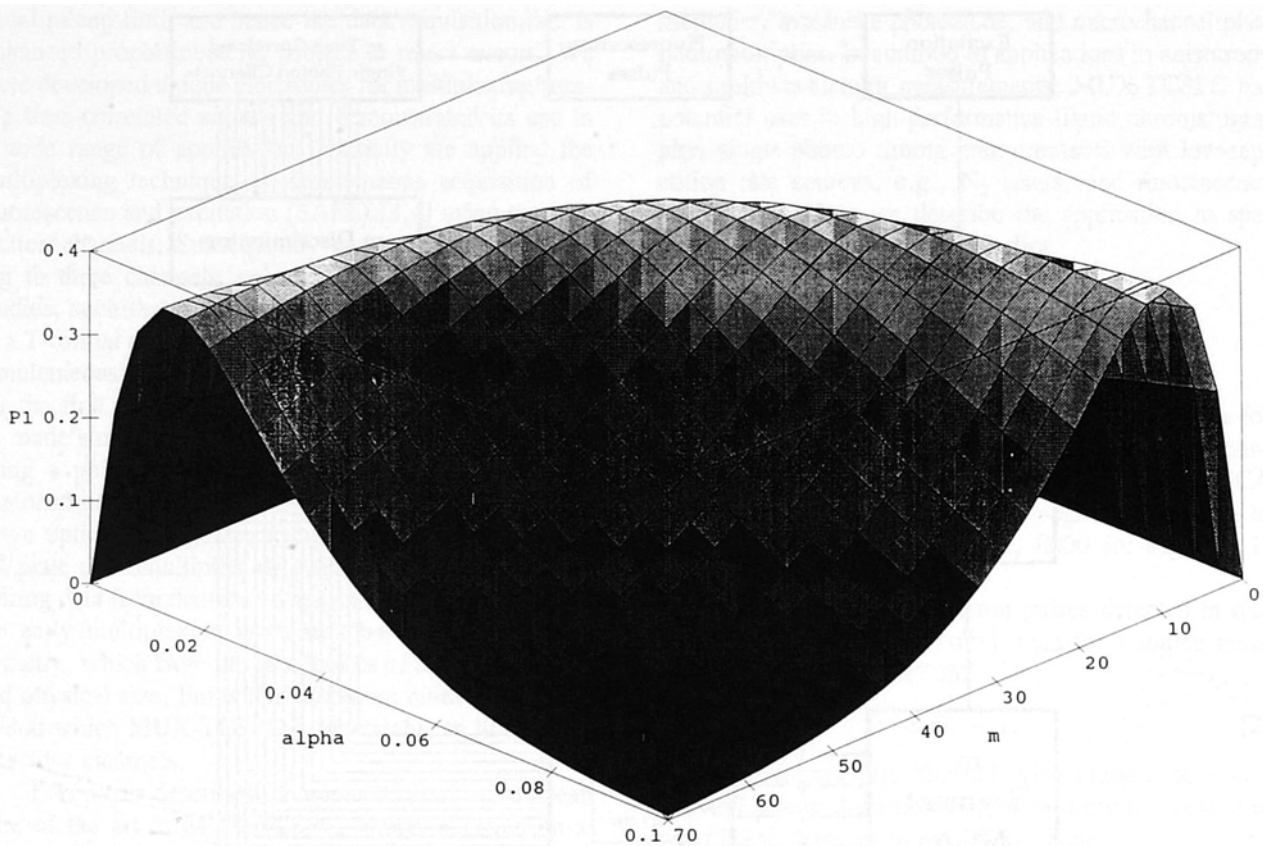Figure 2 plots the contour associated with Eq. (8) in terms of the dependence of the multiplexed detection

Fig. 2. Contour of multiplexed detection probability $P_1(m)$, number of channels m, and "stop"-to-"start" ratio α.

probability $P_1(m)$ on the number of channels m and the stop-to-start rate ratio per channel α. It can be seen from Fig. 2 that even in spite of the necessity to reject counts, the overall detection probability in multiplexing can approach ~0.4, which compares very favorably with the usual probability of 0.01 in simplexed measurements. Figure 2 also shows the operating parameters which are less than optimum, e.g., operating a large number of channels at high α values, which only leads to a high reject rate.

By differentiating Eq. (8) with respect to α, it can be shown that the maximum value of $P_1(m)$ (and hence maximum TAC conversion rate) occurs at

$$\alpha = \frac{1}{m} \qquad (11)$$

Such that the maximum value of $P_1(m)$ is then given by

$$P_1^{max}(m) = \left(1 - \frac{1}{m}\right)^{m-1} \qquad (12)$$

Hence for 16 channels the overall count rate converted by the TAC is maximized at 38% if each channel operates at an α ~6% stop-to-start rate ratio. This is above the α value of ~1% normally used in single-channel measurements, but if the $\alpha = 1\%$ simplex boundary condition is imposed, then $P_1(m)$ will be maximized at its limiting value of ~37% for 100 detection channels.

The theory which we have outlined to describe MUX-TCSPC neglects the effect of electronic dead time in reducing the count rate recorded by the MCA. By far the largest contribution to dead time in any TCSPC system is that of the MCA. For example, a typical MCA dead time of 20 μs would limit the maximum count rate detected to the inverse of this, i.e., 50 kHz. We have developed the multiplexing theory to account for the effect of dead time. These results will be published shortly, but for many practical implementations of MUX-TCSPC dead time effects are not significant, hence we do not consider them further here. Suffice it to say that we have previously tested the multiplexing theory using a pur-

pose-designed pulse generator and found excellent agreement at data rates input to the TAC up to 10 MHz once dead-time effects are considered [16].

At lower count rates the multiplexing theory can be tested independently of the effect of dead time. The data for Fig. 3 were obtained for 16 channels using count rates derived from a flashlamp operating at a 40-kHz start rate, i.e., dead-time effects were negligible. The multiplexing theory is seen to describe the observed count rates well.

MULTIPLEXING APPLICATIONS

The general multiplexing approach described previously has already been successfully demonstrated in a number of important applications including SAFE, anisotropy, and multiwavelength fluorometry. In this paper we apply MUX-TCSPC to two new applications and show how it can produce new insight into the well-known effect of radiative self-absorption in a sample and provide new opportunities with fluorescence lifetime sensors.

Self-Absorption Topography

Figure 4 shows the implementation of MUX-TCSPC which we have used to study self-absorption (also called inner-filter effect or radiative migration) in a solution of
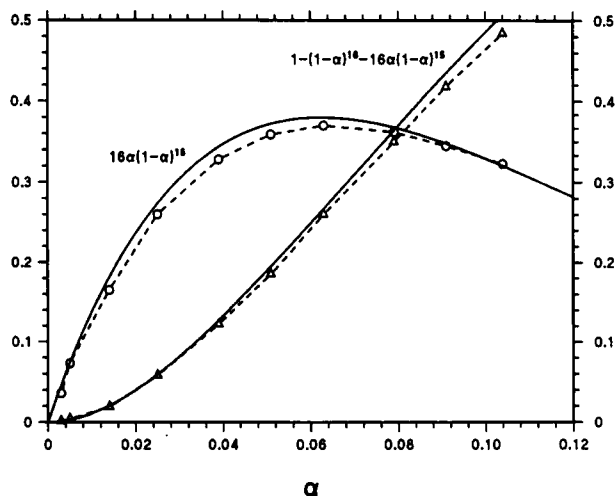

Fig. 4. MUX-TCSPC system used to study self-absorption.

Fig. 3. Measured probabilities for obtaining a multiplexed TAC output $P_1(m)$ 0 and reject event $P_{>1}(m)\triangle$ vs stop-to-start rate ratio α for the case of $m = 16$ channels. The solid lines are the theoretical predictions.
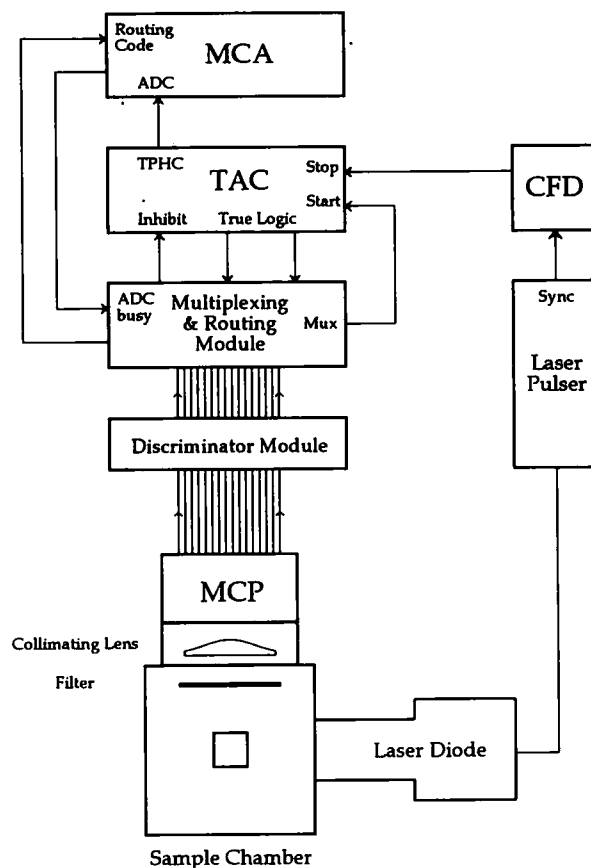
aerated perylene in toluene. The excitation source is a frequency-doubled diode laser (Hamamatsu PLP-01) giving 385-nm pulses of about 28-ps duration at repetition rates up to 10 MHz. The detector used is a 16-anode microchannel plate photomultiplier (MCP-PM); (Hamamatsu R1712U-03) with the photocathodes arranged in a 4 × 4 square array of side 16 mm. The 16 MCP-PM outputs are shaped and timed without further amplification using a 16-leading edge discriminator module (Phillips Scientific 706). The 16 discriminator outputs are connected to a new commercially available multiplexing-routing NIM module (IBH Model 5000MXR) containing the custom-designed IC. The multiplexing-routing module sums the 16 discriminator inputs to provide "start" pulses to the TAC (operated in reverse mode), directs the associated TAC (Ortec 576) conversions to the appropriate MCA (Ortec ADCAM Model 918A) memory segments, generates an enable time window during which routing can occur, and rejects any cross-channel coincidences by inhibiting the TAC. The single-

photon timed measurements are obtained in a reverse "start"–"stop" mode to reduce the TAC dead time at the high laser repetition rates. The decay data are analyzed with the IBH library using a 33 MHz 486DX PC.

As can be seen in Fig. 4 a plano-convex lens, positioned with the sample at its focus, delivers parallel light onto the MCP-PM. Consequently, each detection element of the MCP-PM array will collect fluorescence from a different distribution of point sources along, the diode laser excitation path. In an optically dilute sample we would expect each element of the MCP-PM to give the same fluorescence lifetime. However, our results presented here show how easily MUX-TCSPC resolves changes in the apparent fluorescence lifetime as a function of the detection geometry for the case of self-absorption in an optically dense sample.

The orientation of the MCP-PM detection elements viewing the sample is shown in Fig. 5. This orientation was chosen to maximize the spatial resolution available with the 4 × 4 element array. To begin with we checked the consistency of multiplexed measurements with sim-

plexed measurements taken for each MCP-PM element in turn. This is shown in Table I for a 5 μM solution of perylene in toluene. For all the elements the fluorescence lifetimes agree to better than or equal to 50 ps when recorded using the two methods. However, lifetime variations of up to 300 ps between the elements are observed and attributed to the self-absorption topography.

Table II shows the fluorescence lifetime values obtained at each of the 16 MCP-PM elements as a function of perylene concentration with the cuvette positioned central to the intersecting optical axes. At first glance it is difficult to see any trends or correlations in the data other than the fact that the measured lifetime increases with concentration. This observation has of course been made previously by others. Birks [17] derived the expression for this increase as

$$\tau = \frac{\tau_M}{1 - aq_{FM}} \qquad (13)$$

where τ_M is the molecular fluorescence lifetime (i.e., as measured at infinite dilution), τ the apparent fluorescence lifetime, a the probability of self-absorption (which depends on the overlap of the absorption and fluorescence spectra as well as the pathlength of fluorescence through the sample), and q_{FM} the molecular quantum efficiency. More recently Hirayama and co-workers
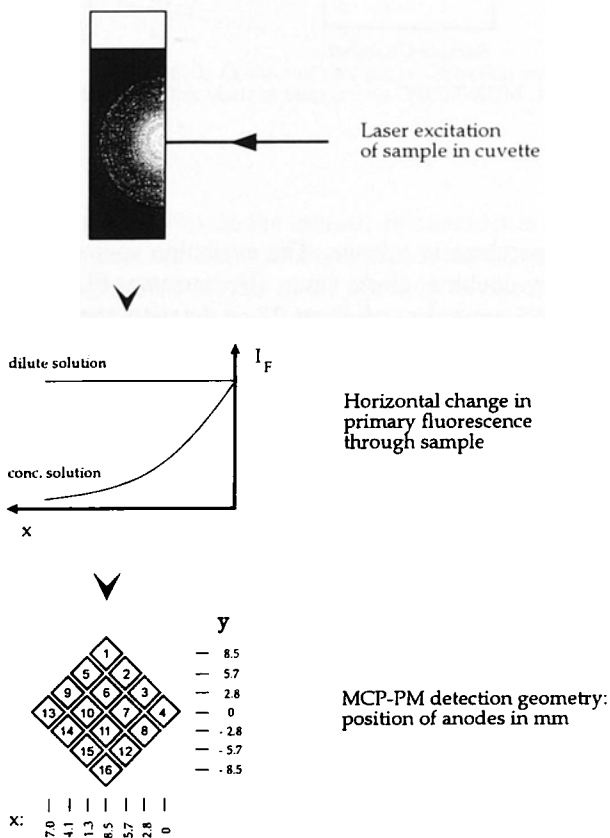

Laser excitation of sample in cuvette

Horizontal change in primary fluorescence through sample

MCP-PM detection geometry: position of anodes in mm

Fig. 5. Multianode MCP orientation for viewing the sample.

Table I. Comparison of Simplexed and Multiplexed MCP-PM Measurements of the Fluorescence Lifetime τ of 5 μM Perylene in Toluene

MCP-PM element	Simplexed τ (ns)	Multiplexed Mean τ (ns)	Multiplexed $\pm\ d\tau$ (ns)
1	4.27	4.26	0.03
2	4.21	4.26	0.03
3	4.20	4.23	0.02
4	4.07	4.11	0.02
5	4.26	4.28	0.04
6	4.18	4.23	0.01
7	4.22	4.20	0.03
8	4.04	4.06	0.05
9	4.27	4.25	0.12
10	4.16	4.21	0.01
11	4.11	4.12	0.02
12	4.00	4.00	0.01
13	4.34	4.29	0.07
14	4.15	4.15	0.02
15	3.95	3.98	0.02
16	4.19	4.12	0.05

Table II. Multiplexed Multianode MCP-PM Fluorescence Lifetimes at Different Perylene Concentrations

MCP-PM element	τ (ns)						
	1.5 μM	15 μM	75 μM	0.15 mM	0.32 mM	0.75 mM	1.5 mM
1	4.09	4.68	5.14	5.31	5.57	5.75	6.11
2	3.96	4.54	4.99	5.18	5.59	6.00	6.91
3	3.95	4.44	4.92	5.12	5.39	5.54	5.56
4	3.88	4.28	4.79	4.92	5.07	5.22	5.30
5	3.94	4.50	4.98	5.12	5.37	5.58	5.62
6	3.93	4.45	4.84	5.10	5.72	6.48	6.91
7	3.99	4.46	4.84	5.08	5.48	5.67	5.63
8	3.90	4.30	4.72	4.89	5.12	5.29	5.34
9	3.93	4.42	4.87	5.07	5.45	5.73	5.90
10	3.87	4.31	4.75	5.00	5.50	6.13	6.71
11	3.86	4.26	4.65	4.87	5.27	5.70	5.79
12	4.02	4.51	4.63	5.05	5.64	5.95	5.61
13	3.97	4.47	4.90	5.13	5.91	6.95	6.96
14	3.95	4.40	5.04	5.02	5.69	6.58	7.14
15	4.08	4.64	5.06	5.41	6.09	6.35	6.57
16	3.86	4.28	4.66	4.89	5.74	6.31	6.54

[18,19] have treated the measured decay in terms of a series of convolution integrals representing the successive reabsorptions to give an observed decay form [18,19]

$$I(t) = \sum_{i=1}^{n} a_i F_i(t) \qquad (14)$$

where $F_1(t) = \ell(t) \otimes \exp(-t/\tau_M)$, $F_i(t) = F_{i-1}(t) \otimes \exp(-t/\tau_M)$; $\ell(t)$ represents the instrumental response function, and a_i is a measure of the contribution of the ith component to the emission.

The apparent fluorescence lifetime τ can then be related to the true fluorescence lifetime τ_M by the average number of transfer steps $\langle n \rangle$ such that [18,19]

$$\tau = \langle n \rangle \, \tau_M \qquad (15)$$

For values of $\langle n \rangle$ < 1.1 Hirayama and co-workers [18,19] observed monoexponentiality in the decay, but above this value a convex decay profile and a rise time were obtained. The wavelength dependence of self-absorption has also been studied in detail by Martinho and co-workers [20].

Figure 6 demonstrates the appearance of a rise time and convex decay in a 1.5 mM solution of perylene compared to the monoexponentiality of a 1.5 μM solution measured in element 13 of the MCP PM. The corresponding lifetimes we observed are 6.9 and 3.97 ns, respectively.
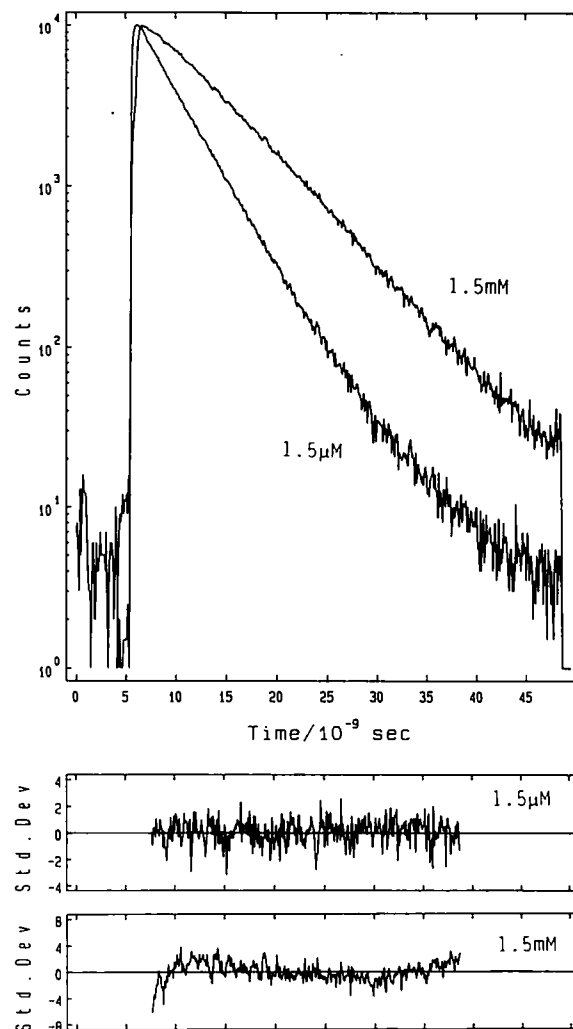

Fig. 6. Fluorescence decays measured with MCP-PM element 13 at 1.5 μM and 1.5 mM perylene concentrations. A reconvoluted monoexponential fit to these data gave χ^2 values of 1.21 and 2.33, respectively.

Returning now to the spatial dependence of the apparent fluorescence lifetime, it is noted that both Eq. (13) and Eq. (14) predict this through the parameter a. A general theoretical analysis of the spatial dependence is extremely difficult, if not impossible, to achieve. However, from a practical standpoint a fuller appreciation of the salient geometrical influence would be most helpful, and in this respect multiplexing multianode MCP signals allows the observation of a more complete time-domain fluorescence topography than has hitherto been possible. To help us in identifying trends we have sorted the MCP-PM signals shown in Table II into vertical (i.e., perpendicular to the axis of excitation) and horizontal

(i.e., along the axis of excitation) elements and the results shown in Figs. 7 and 8 as a function of displacement. Only for perylene concentrations ≥ 0.32 mM is an increase in lifetime observed with horizontal displacement away from the excitation face of the cuvette. We attribute this to the dominant influence of radiative migration on the fluorescence signal detected, as the penetration depth is reduced at such concentrations. The results clearly show how self-absorption effects can be minimized by limiting observation to the excitation axis if a 90° geometry is to be used. Contrastingly, the vertical analysis shown in Fig. 8 shows changes in the lifetime with displacement at all concentrations. This we attribute to the preferential detection of the "off-excitation axis" signal above and below the laser beam. In
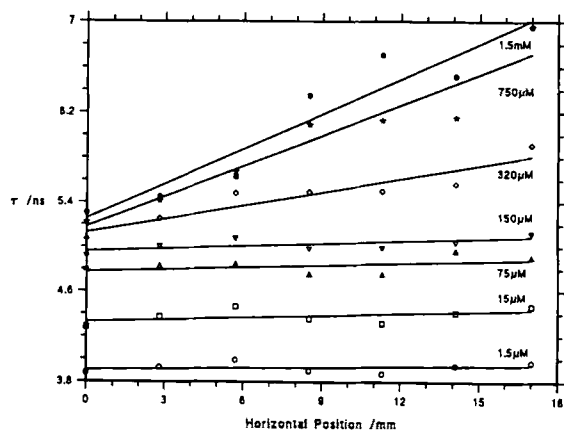
fact the data in Fig. 8 show a common dip in all the curves at -3 mm, which we attribute to the arbitrary vertical position of the laser beam. The reduction in fluorescence lifetime at the extreme displacement in some cases shown in Fig. 8 might well be due to internal reflection in the cuvette. Figure 9 correlates the fluorescence lifetime gradient with horizontal displacement $d\tau/dx$ and the $1/e$ optical penetration depth [i.e., $\epsilon^{-1}(\lambda)c^{-1}$] using the extinction coefficient $\epsilon(385$ nm$) = 8000$ mol cm^{-1}. The sharp increase in $d\tau/dx$ occurs when the penetration depth becomes less than the sample width observed by the detector (in this case, 0.8 cm) such that radiative migration is the dominant source of the detected fluorescence. Figure 10 mirrors the $d\tau/dx$ trend in terms of the mean χ^2 values over all the data associated with Table II when fitted to a monoexponential decay

Fig. 7. Horizontal analysis of multiplexed MCP-PM data for the fluorescence decay of perylene at different concentrations.

Fig. 9. Penetration depth $\epsilon^{-1}(\lambda)c^{-1}$ and fluorescence lifetime gradient $d\tau/dx$ as a function of perylene concentration.

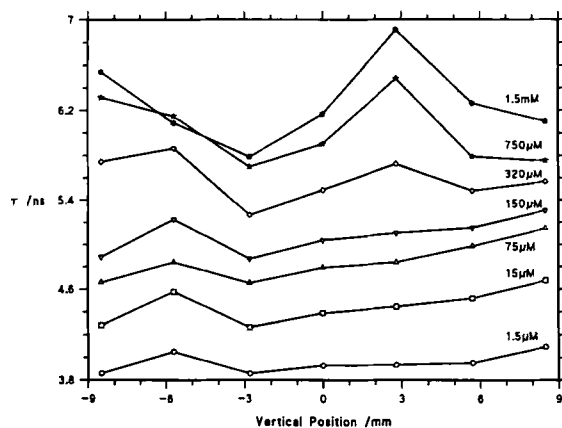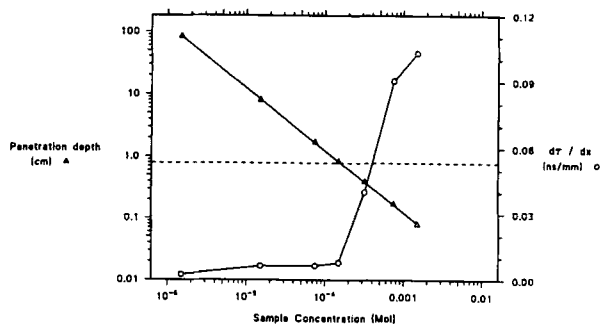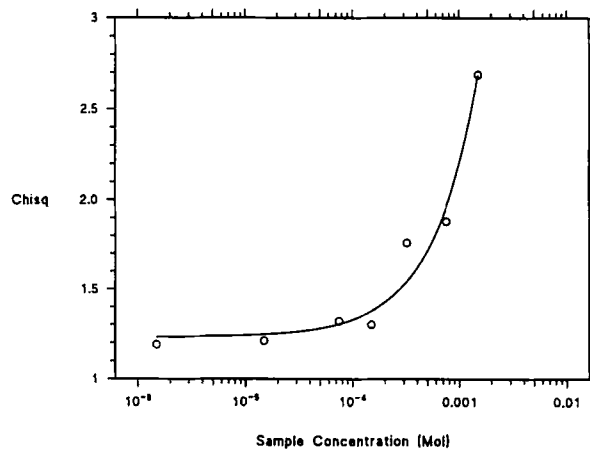**Fig. 8.** Vertical analysis of multiplexed MCP-PM data for the fluorescence decay of perylene at different concentrations.

Fig. 10. Mean χ^2 values obtained with horizontal MCP-PM elements when fitting varying concentrations of perylene to a monoexponential decay model.

function. Hence Fig. 10 approximates to the χ^2 trend which would be detected by a single-anode MCP-PM, i.e., without the spatial resolution afforded by multiplexing multianode signals.

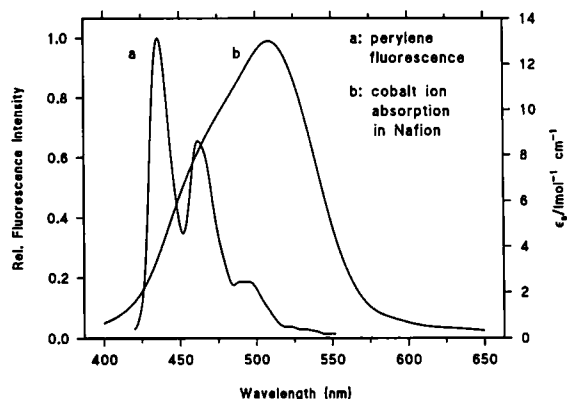The results in this section serve to demonstrate the

Fig. 11. Fluorescence spectrum of perylene and absorption spectrum of Co^{2+} ions in a Nafion polymer membrane.
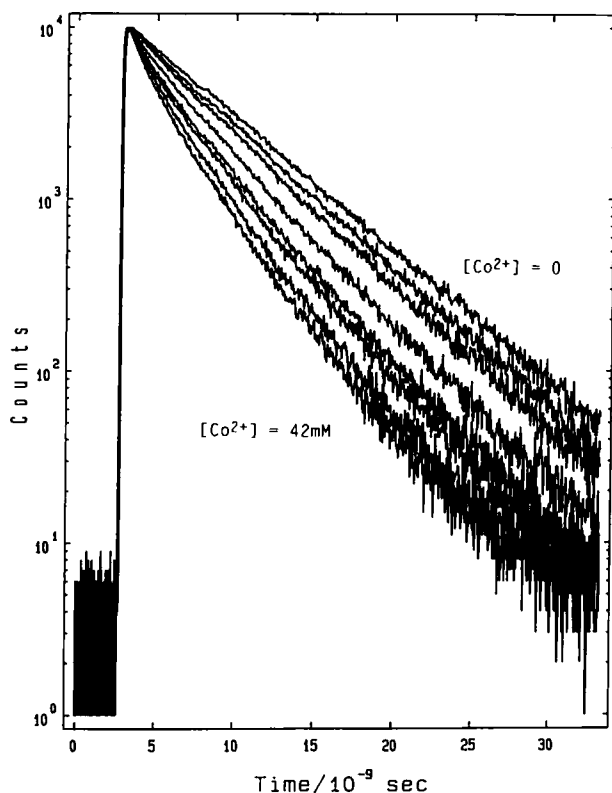

Fig. 12. Fluorescence decay of perylene in Nafion at Co^{2+} concentrations on the film of between 3 and 42 mM.

Table III. Fluorescence Decay Analysis of Perylene in Nafion Quenched by Co^{2+} Ions

| [Co²⁺] (M)	1 exponential		3D Förster fit			
	τ (ns)	χ²	τ (ns)	γ	χ²	[Co²⁺]_calc (M)
0	5.55	1.26	5.61	0.010	1.24	
0.003	5.29	1.48	5.54	0.052	1.28	0.008
0.006	5.15	1.74	5.48	0.077	1.31	0.012
0.009	4.92	1.84	5.29	0.077	1.37	0.012
0.012	4.76	2.30	5.32	0.120	1.33	0.019
0.015	4.25	3.60	5.06	0.190	1.27	0.030
0.018	4.11	3.80	4.93	0.200	1.24	0.032
0.021	4.09	3.94	4.96	0.210	1.17	0.033
0.024	3.50	5.97	4.79	0.310	1.21	0.049
0.027	3.53	5.39	4.63	0.290	1.36	0.046
0.030	3.38	6.66	4.64	0.344	1.15	0.055
0.033	3.36	6.27	4.59	0.347	1.12	0.055
0.036	2.97	7.77	4.39	0.430	1.28	0.068
0.042	2.74	9.55	4.47	0.539	1.17	0.086
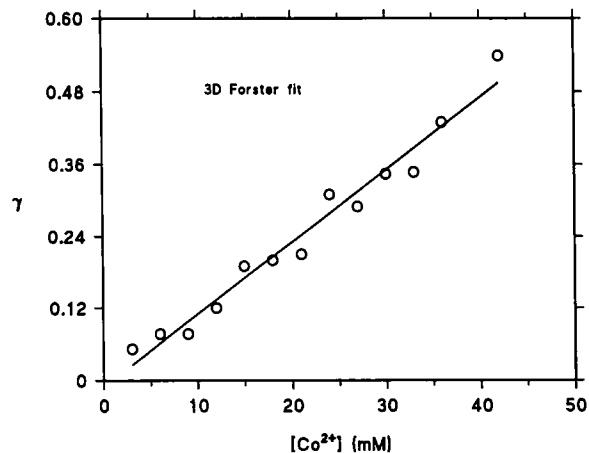
Fig. 13. Dependence of Förster parameter γ on Co^{2+} ion concentration.

power of MUX-TCSPC in bringing all the advantages of TCSPC to bear on spatial-dependent fluorescence kinetics. Other such examples where MUX-TCSPC should be useful include fluorescence microscopy [21], angle-resolved fluorescence depolarization measurements [22], and total internal reflection fluorescence spectroscopy [23].

Multiplexed Sensor Networks

Our final application of MUX-TCSPC concerns its potential for handling fluorescence decay data from a distributed network of fluorescence sensors coupled to
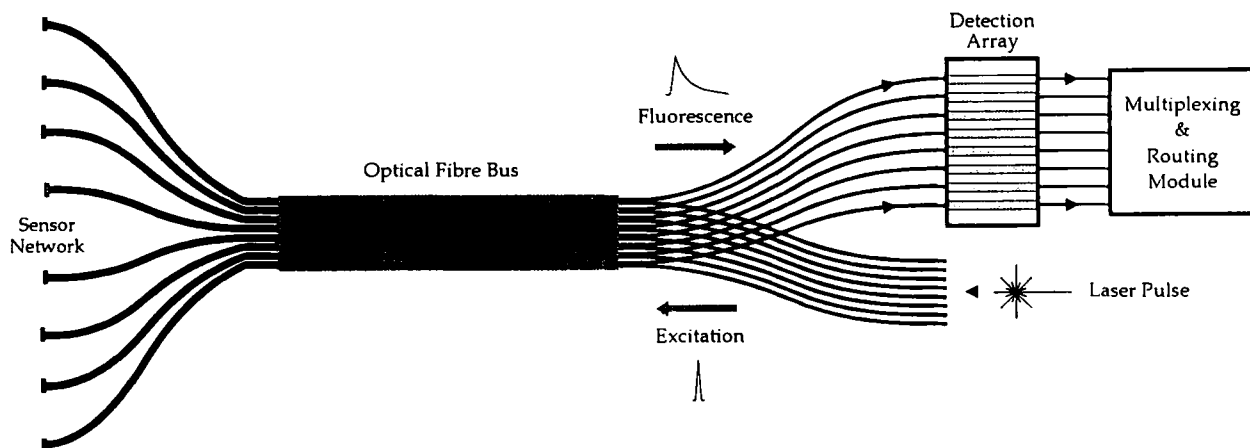
Fig. 14. Multiplexed sensor network.

single-photon timing detectors (e.g., MCP-PM) via optical fibers.

In recent years the opportunities for fluorescence lifetime-based sensors over their steady-state equivalents have started to be appreciated. Advantages include the lack of influence of fluorophore concentration, higher measurement precision, simple calibration, and lower susceptibility to systematic errors. Nevertheless, by and large the vast majority of fluorescence lifetime-based sensor research has utilized phase-modulation techniques, chiefly because of the speed of measurement and low cost [24]. In addition, the photophysical mechanism behind most proposed fluorescence quenching sensors has been that of Stern–Volmer collisional quenching [25,26], where the concentration of quencher [Q] can be determined from

$$\frac{\tau_M}{\tau} = \frac{\phi_M}{\phi} = 1 + \tau_M k_Q[Q] \qquad (16)$$

where τ_M, τ and ϕ_M, ϕ relate to the lifetime and quantum yield in the absence and presence of quenching and k_Q is the quenching constant. Unfortunately the use of Eq. (16) is limited in mixtures of quenchers because of the lack of specificity, i.e., all collisional quenchers reduce the fluorescence lifetime to some extent. In recent years we have been researching the possibility of making fluorescence lifetime sensors based on quenching due to Förster dipole–dipole nonradiative energy transfer. There are a number of potential advantages of this approach including specificity due to the requirement for spectral overlap between the sensor fluorescence and the quencher absorption, the long-range nature of the quenching (up

to 100 Å in some cases) allowing the fluorophore to be buried (and hence protected) in the sensor matrix, and obviation of the effect of collisional quenching due to the transient nature of energy transfer.

The MUX-TCSPC technique is clearly appropriate for acquiring data from a distributed sensor array where each sensor might be tuned to detect a different analyte and where high time resolution is required to observe the Förster transient. We first became aware of the possibility of fabricating a Förster-type sensor when we found that energy transfer from perylene to cobalt (Co^{2+}) ions across the aqueous interface of a lipid bilayer membrane could be described well by Förster's model once donor–donor effects had been corrected [27]. Subsequently we observed differences in the quenching mechanism in lipid bilayers for different metal ions [28] and thus proposed the new type of sensor [29].

The fluorescence response function for Förster energy transfer in three dimensions is [30]

$$I(t) = I_o \exp\left[-\frac{t}{\tau_M} - 2\gamma \sqrt{\frac{t}{\tau_M}} \right] \qquad (17)$$

where

$$\gamma = [Q]/C_{AO} \qquad (18)$$

C_{AO} being the critical acceptor concentration, which can be determined either by calibration or from the spectral overlap of fluorophore (donor) emission and quencher (acceptor) absorption. Equations (17) and (18) together thus afford an opportunity for determining the analyte

concentration [Q] directly from the analysis of the fluorescence decay.

As the second stage of our research into energy transfer-based sensors, we encapsulated perylene in the perfluorosulfonate polymer Nafion (supplied by Aldrich in sheets) and sought to replicate the classic Förster quenching of perylene by Co^{2+} ions. Nafion is an anionic polymer which swells in aqueous solution due to microscopic cavities which are analogous to inverse micelles [31]. The Nafion films were first cleaned by boiling in concentrated nitric acid for 30 min and then purified in water for 1 h. The films were doped with perylene from a methanol solution. Fluorescence decay measurements were obtained using the instrument shown in Fig. 4 with an instrumental FWHM of about 100 ps. The fluorescence spectrum of perylene in Nafion and the absorption spectrum of Co^{2+} ions in Nafion are shown in Fig. 11. The perylene fluorescence spectrum is shifted 8 nm toward the blue compared with that in lipid bilayers. The presence of the 0–0 band indicates the absence of radiative migration. Nevertheless, significant overlap with the Co^{2+} absorption is evident. Figure 12 shows the quenching of the perylene fluorescence decay with increasing Co^{2+} concentration. Table III shows the three-dimensional Förster analysis of these data and compares the Co^{2+} concentration on the film with that determined from analysis of the fluorescence decay. The correlation is promising and it should be noted that, given the ion-harvesting properties of the Nafion, many orders of magnitude reduction in solution concentration below that on the film can be detected. The linear dependence of γ on Co^{2+} concentration is shown in Fig. 13. The fact that this line passes through the origin and the monoexponential decay of perylene in the absence of Co^{2+} ions together indicate the lack of perylene–perylene nonradiative energy transfer and hence the absence of perylene clustering [27]. The overall level of agreement provides a good starting point given the extent to which the kinetic model we are using is designed for a homogeneous system, which the Nafion environment most certainly is not (a two-dimensional Förster treatment making little difference), and takes no account of collisional quenching, which the decrease in τ with [Co^{2+}] shows is occurring. From the slope in Fig. 13 the interaction radius is found to be 17.5 Å, a little different, but not too far away, from the theoretical value of 14.2 Å determined from the spectral overlap integral in Nafion.

Clearly, considerable work is required to optimize energy transfer-based metal ion sensors. The technique can be refined with other polymers, fluorophores, etc., once the quenching kinetics are better modeled. Should fluorescence sensors based on TCSPC prove to be useful, then the multiplexing approach described here will undoubtedly enhance their capability considerably by allowing sensor networking to be handled simply at a minimum cost while preserving the high time resolution. Figure 14 shows one possible network implementation which would permit the simultaneous monitoring of a range of analytes.

ACKNOWLEDGMENTS

REFERENCES

1. D. V. O'Connor and D. Phillips (1984) *Time-Correlated Single-Photon Counting*, Academic Press, New York.
2. D. J. S. Birch and R. E. Imhof (1991) in J. R. Lakowicz (Ed.), *Topics in Fluorescence Spectroscopy, Vol. 1*, Plenum, New York, pp. 1–95.
3. International Patent No. WO 85/03352.
4. D. J. S. Birch, R. E. Imhof, and A. Dutch (1984) *Rev. Sci. Instrum.* **55**, 1255–1264.
5. D. J. S. Birch, A. S. Holmes, J. R. Gilchrist, R. E. Imhof, S. M. Al-Alawi, and B. Nadolski (1987) *J. Phys. E Sci. Instrum.* **20**, 471–473.
6. D. J. S. Birch, R. E. Imhof, and C. Guo (1988) *J. Photochem. Photobiol A Chem.* **42**, 223–231.
7. D. J. S. Birch, A. S. Holmes, R. E. Imhof, B. Z. Nadolski, and K. Suhling (1988) *J. Phys. E Sci. Instrum.* **21**, 415–417.
8. D. J. S. Birch, A. S. Holmes, R. E. Imhof, and J. Cooper (1988) *Chem. Phys. Lett.* **148**, 435–444.
9. A. Sanderson, A. S. Holmes, D. McLoskey, D. J. S. Birch, and R. E. Imhof (1993) *SPIE Proc.* **1885**, 466–477.
10. D. J. S. Birch, A. Sanderson, A. S. Holmes, D. McLoskey, and R. E. Imhof (1993) *Meas. Sci. Tech.* **4**, 797–799.
11. Ph. Wahl (1983) in R. B. Cundall and R. E. Dale (Eds.), *Time-Resolved Fluorescence Spectroscopy in Biochemistry and Biology*, Plenum Press, New York, pp. 483–495.
12. G. Hazan, A. Grinvald, M. Maytal, and I. Z. Steinberg (1974) *Rev. Sci. Instrum.* **45**, 1602–1604.
13. H. Dreeskamp, T. Salthammer, and A. G. E. Läfer (1989) *J. Luminesc.* **44**, 161–165.
14. R. W. Wijnaendts van Resandt, R. H. Vogel, and S. W. Provencher (1982) *Rev. Sci. Instrum.* **53**, 1392–1397.
15. R. W. Wijnaendts van Resandt (1983) *Chem. Phys. Lett.* **95**, 205–208.
16. D. J. S. Birch, K. Suhling, A. S. Holmes, and R. E. Imhof (1990) *SPIE Proc.* **1204**, 26–34.
17. J. B. Birks (1970) *Photophysics of Aromatic Molecules*, Wiley-Interscience, New York, p. 92.
18. Y. Sakai, M. Kawahigashi, T. Minami, T. Inoue, and S. Hirayama (1989) *J. Luminesc.* **42**, 317–324.
19. A. D. Scully, A. Matsumoto, and S. Hirayama (1991) *J. Luminesc.* **157**, 253–269.
20. J. M. G. Martinho, A. L. Macanita, and M. N. Berberan-Santos (1989) *J. Chem. Phys.* **90**, 53–59.
21. S. Hirayama (1992) *Progress in Photochemistry and Photophysics, Vol. VI*, pp. 1–42.

22. H. Van Langen, G. Van Ginkel, and Y. K. Levine (1989) *Chem. Phys.* **130**, 271–278.
23. M. Yanagimachi, M. Toriumi, and H. Masuhara (1992) *Appl. Sec.* **46**, 832–840.
24. J. R. Lakowicz, H. Szmacinski, and K. W. Berndt (1992) *SPIE* **1648**, 150–163.
25. W. A. Wyatt, F. V. Bright, and G. M. Hieftje (1987) *Anal. Chem.* **59**, 2272–2276.
26. M. E. Lippitsch, J. Pusterhofer, M. J. P. Leiner, and O. S. Wolfbeis (1988) *Anal. Chim. Acta.* **205**, 1–6.

27. A. S. Holmes, D. J. S. Birch, K. Suhling, R. E. Imhof, T. Salthammer, and H. Dreeskamp (1991) *Chem. Phys. Lett.* **186**, 189–194.
28. D. J. S. Birch, K. Suhling, A. S. Holmes, T. Salthammer, and R. E. Imhof (1992) *SPIE* **1640**, 707–718.
29. D. J. S. Birch, K. Suhling, A. S. Holmes, T. Salthammer, and R. E. Imhof (1993) *Pure Appl. Chem.* **65**, 1687–1692.
30. Th. Förster (1949) *Z. Naturforsch.* **4a**, 321–327.
31. E. P. Niu, K. P. Ghiggino, T. A. Smith, and W. H. Mau (1990) *J. Luminesc.* **46**, 191–199.